Comparative study on mouse models of acute exacerbation of pulmonary fibrosis

XU YE[1,2*], MINGRUI ZHANG[3*], MENGYING LIU[1], HUIHUI ZHU[3], XIAOLING YE[1], CHENG JIANG[3], QI LI[3], XINMEI HUANG[1,4] and MENGSHU CAO[1,3-5]

[1]Department of Respiratory and Critical Care Medicine, Nanjing Drum Tower Hospital, Affiliated Hospital of Medical School, Nanjing University, Nanjing, Jiangsu 210008, P.R. China; [2]Department of Respiratory and Critical Care Medicine, Nanjing First Hospital, Nanjing University of Chinese Medicine, Nanjing, Jiangsu 210008, P.R. China; [3]Department of Respiratory and Critical Care Medicine, Nanjing Drum Tower Hospital, Drum Tower Clinical Medical College, Nanjing University of Chinese Medicine, Nanjing, Jiangsu 210008, P.R. China; [4]Nanjing Institute of Respiratory Diseases, Department of Respiratory and Critical Care Medicine, Nanjing Drum Tower Hospital, Affiliated Hospital of Medical School, Nanjing University, Nanjing, Jiangsu 210008, P.R. China; [5]Department of Respiratory and Critical Care Medicine, Nanjing Drum Tower Hospital, Drum Tower Clinical Medical College, Nanjing Medical University, Nanjing, Jiangsu 210008, P.R. China

Received August 10, 2025; Accepted June 24, 2026

DOI: 10.3892/etm.2026.13248

Abstract. The etiology and underlying mechanisms of acute exacerbation of idiopathic pulmonary fibrosis (AE-IPF) remain poorly understood. Although several animal models have been developed to study AE-IPF, a systematic evaluation and comparison of these models has not yet been reported. In the present study, PF was induced in mice by a single intratracheal administration of bleomycin (BLM). On day 14 after the initial BLM challenge, AE-PF in mice was induced by intratracheal re-challenge with replication-deficient adenoviral vectors (ADV), lipopolysaccharide (LPS) or a second dose of BLM. Micro-chest computed tomography (CT) was performed on day 20, and blood, bronchoalveolar lavage fluid (BALF) and lung tissue samples were collected after sacrifice on day 21. Compared with mice receiving a single dose of BLM alone, all three AE-PF groups exhibited significant body weight loss and increased mortality (with the highest mortality in the LPS group), as well as more extensive lung injury on CT. Histopathological scores for inflammation and fibrosis, hydroxyproline content and expression levels of fibrotic markers (fibronectin, collagen I, α-smooth muscle actin and MMP7) were significantly elevated in the AE-PF groups. Inflammatory cytokines (IL-6, IL-1β and TNF-α) were markedly increased in both serum and BALF. Furthermore, the AE-PF models showed downregulation of alveolar epithelial cell markers (E-cadherin and pro-surfactant protein C) and a significant increase in apoptotic activity. Notably, fibrosis progression was more severe in the ADV and two-dose BLM groups than in the LPS group. Taken together, these findings indicate that all three triggers can induce AE-PF through enhanced apoptosis, inflammation and fibrosis. These results support the use of day 14 re-challenge as a standardized model for AE-PF. Among the three models, the ADV-induced AE-PF model may serve as a particularly suitable platform for investigating the pathogenesis of acute exacerbations in idiopathic pulmonary fibrosis.

Correspondence to: Professor Mengshu Cao, Department of Respiratory and Critical Care Medicine, Nanjing Drum Tower Hospital, Affiliated Hospital of Medical School, Nanjing University, 321 Zhongshan Road, Nanjing, Jiangsu 210008, P.R. China
E-mail: mengshucao@nju.edu.cn

*Contributed equally

Abbreviations: ADV, adenoviral vectors; AEC, alveolar epithelial cells; AE, acute exacerbation; AE-PF, acute exacerbation of pulmonary fibrosis; AE-IPF, acute exacerbation of idiopathic pulmonary fibrosis; ARDS, acute respiratory distress syndrome; BALF, bronchoalveolar lavage fluid; BLM, bleomycin; IPF, idiopathic pulmonary fibrosis; LPS, lipopolysaccharide; α-SMA, α-smooth muscle actin

Key words: pulmonary fibrosis, acute exacerbation, animal models, adenovirus

Introduction

Idiopathic pulmonary fibrosis (IPF) is a chronic, fibrosing interstitial pneumonia of unknown etiology (1). A subset of patients with IPF may experience acute exacerbations (AE), diagnosed based on established clinical criteria: A previous or concurrent diagnosis of IPF; acute worsening of dyspnea (typically over <1 month); high-resolution computed tomography findings of new bilateral ground-glass opacities and/or consolidation superimposed on a usual interstitial pneumonia pattern; and exclusion of cardiac failure or fluid overload (2). These exacerbations lead to acute and clinically notable respiratory deterioration. The annual incidence of AE-IPF ranges from 5 to 10% (3,4), with mortality rates between 56 and

100% (5). Without lung transplantation, the median survival time after an AE is 3-4 months (6,7). Current international guidelines provide only a weak recommendation for glucocorticoid therapy in AE-IPF, and lung transplantation remains the only effective long-term treatment for these critically ill patients (1,8-10).

The etiology of AE-IPF is multifactorial, including bacterial or viral infections, drug toxicity, aspiration, intrinsic defects and surgical-related injuries (10-12). Viral infection often serves as an initiating event (13). Research suggests that latent viruses can modify the secretory phenotype of lung cells, promoting a pro-fibrotic environment even when the latent viral load is low or after mRNA COVID-19 vaccination (14-16). Other studies have shown that the bacterial load in bronchoalveolar lavage fluid (BALF) from patients with AE-IPF is considerably higher when compared with that from stable patients (13). Nevertheless, the exact pathogenesis of AE-IPF remains unclear. Studies indicate that it may involve increased epithelial cell apoptosis and excessive inflammatory responses (17-19). Notably, type 2 alveolar epithelial cells (AEC2s), which function as alveolar stem cells, exhibit heightened apoptosis and loss of self-renewal capacity, playing a pivotal role in pulmonary fibrosis progression (20-22).

To investigate the mechanisms of AE-IPF, several animal models have been established. These models typically involve initial treatment with bleomycin (BLM) or other toxic agents to induce pulmonary fibrosis via alveolar epithelial cell injury (23,24); alternatively, TGF-β1 transgenic mice are used to directly establish pulmonary fibrosis (25). Subsequently, mice are challenged with bacterial, viral or chemical agents to trigger an AE of pulmonary fibrosis (AE-PF) (18,19,23,26). This approach leads to notable alveolar damage, including epithelial cell shedding, widening of the alveolar septa, extensive inflammatory cell infiltration and increased collagen deposition (18,19,27). However, published AE-PF models vary considerably in the choice of agents and the timing of the AE-inducing challenge (17). For example, some models use more toxic agents (24,26), and in certain studies, the AE trigger is administered as early as day 7 after BLM treatment, when lung inflammation is most pronounced but clear fibrosis has not yet developed (27,28). In other studies, AE is induced on day 21, when the fibrotic changes are fully established, a reasonable approach. Nevertheless, fibrosis in the BLM model begins to resolve spontaneously around day 28, so observation at day 35 may yield inaccurate results because natural resolution could confound the assessment of AE effects (29). Moreover, the pathological changes in lung tissue across these models are inconsistent; some show marked destruction of alveolar architecture and significant fibrosis, while others predominantly exhibit inflammation (30,31).

Because the intratracheal BLM mouse model remains the most widely used model of pulmonary fibrosis according to international guidelines published in 2017 (7), the present study established pulmonary fibrosis by intratracheal BLM injection on day 0. On day 14 after the initial BLM treatment, when fibrotic changes are more evident, mice were rechallenged with replication-deficient adenoviral vectors (ADV), lipopolysaccharide (LPS) or a second dose of BLM. The present study systematically compared the pathophysiological features of these three AE-PF models and evaluated their suitability as experimental platforms for investigating the mechanisms underlying acute exacerbations in patients with IPF.

Materials and methods

Animals. Wild-type male C57BL/6 mice (aged 6-8 weeks; weighing 22.3-25.1 g) were obtained from Jiangsu Gempharmatech Co., Ltd. The animals were housed under a 12-h light/dark cycle with controlled humidity (50±15%) and temperature (22±2˚C), with food and water provided ad libitum. Animal health and behavior were assessed twice daily (9:00 AM and 5:00 PM) throughout the study. Humane endpoints were predefined as: i) Body weight loss >30% of initial weight, ii) hunched posture, iii) piloerection, iv) labored breathing or v) inability to reach food or water. Humane endpoints were predefined; however, no animals met these criteria during the study and were euthanized accordingly. All surviving animals were euthanized at the experimental endpoint for tissue collection. All efforts were made to minimize suffering and distress. No analgesics or anesthetics were used during the disease course to avoid interference with inflammatory and fibrotic responses, except for the intratracheal instillation procedure.

A total of 75 mice (15 per group) were initially assigned to the five groups: control (Ctrl), BLM, BLM+ADV, BLM+LPS and BLM+BLM. On day 0, mice in the Ctrl group received an intratracheal injection of 50 μl PBS, whereas mice in the four BLM-treated groups received intratracheal BLM (3 mg/kg in 50 μl PBS; Nippon Kayaku Co., Ltd.). For intratracheal instillations, mice were briefly anesthetized with isoflurane (3% for induction; 1.5% for maintenance) delivered via a nose cone. During the first 14 days following BLM administration, three mice died in each of the four BLM-treated groups, leaving 12 mice per group prior to the second challenge on day 14. On day 14, mice in the Ctrl and BLM groups received an intratracheal injection of 50 μl PBS. Mice in the AE groups (BLM+ADV, BLM+LPS and BLM+BLM) received, respectively: ADV ($1x10^8$ PFU in 50 μl PBS; cat. no. OP0524; OBiO Technology (Shanghai) Corp.), LPS (1 mg/kg in 50 μl PBS; cat. no. L2880-10 MG; *Escherichia coli* O55:B5; MilliporeSigma) or a second dose of BLM (3 mg/kg in 50 μl PBS). No further mortality was observed in the BLM group after day 14 (12 mice survived to day 21). By contrast, mortality occurred in all three AE groups, with final survival numbers of 8 (BLM+ADV), 6 (BLM+LPS) and 8 (BLM+BLM) mice, respectively, as shown in Fig. 1C. All mortalities were attributed to respiratory distress secondary to exacerbated lung injury.

On day 20, mice underwent chest micro-computed tomography (micro-CT) imaging. On day 21, the animals were euthanized by intraperitoneal injection of sodium pentobarbital (150 mg/kg). Mortality was confirmed by cessation of heartbeat and respiration, as well as lack of response to toe pinch. Samples of lung tissue, BALF and peripheral blood were then collected (Fig. 1A). All experimental protocols were approved by the Ethics Committee of Nanjing Drum Tower Hospital, Nanjing University Medical School (Nanjing, China; approval no. 2016-160-01).

Assays of hydroxyproline content of lung tissue. Lung tissue samples (50 mg) were precisely weighed and recorded.

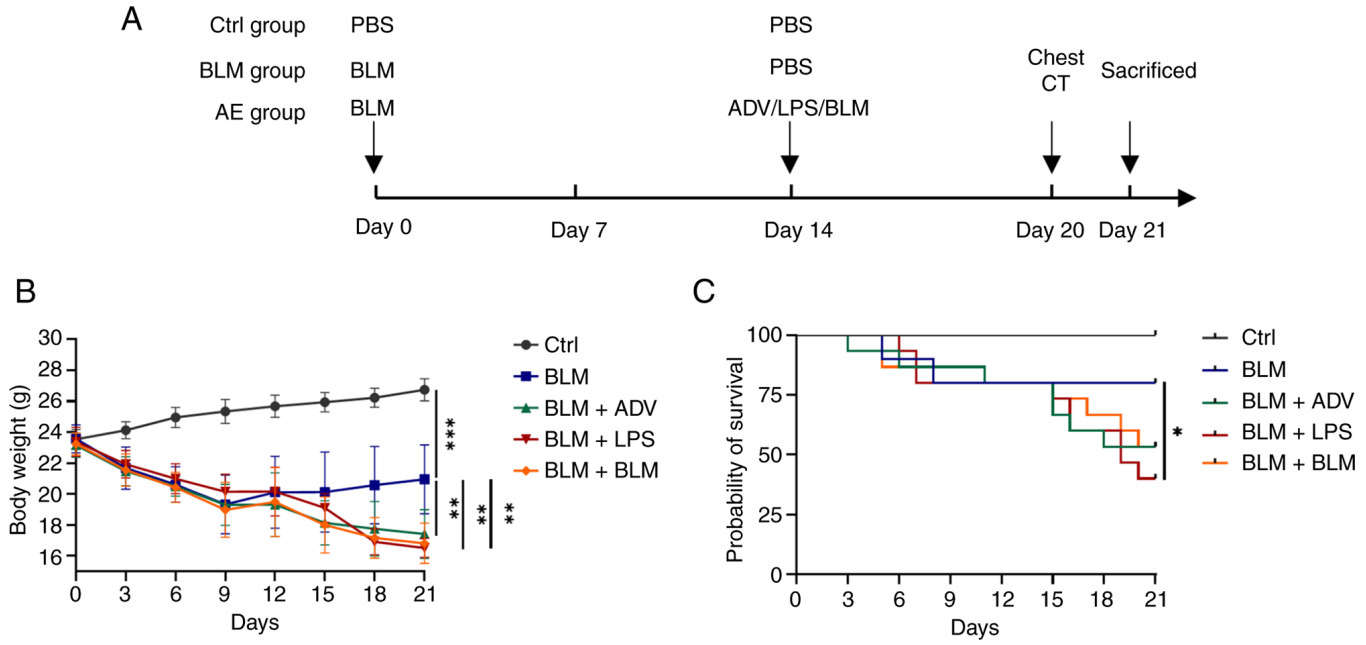

Figure 1. Mouse models of AE-PF. (A) Flow chart of AE-PF mouse models. An intratracheal injection of BLM was performed on day 0, followed by a second intratracheal injection of ADV, LPS or an additional dose of BLM on day 14. (The mice were randomly divided into Ctrl group, BLM group and three AE groups. AE groups include three subgroups: BLM+ADV group, BLM+LPS group and BLM+BLM group. (B) The weight changes over 21 days. The weights of mice in three AE groups were significantly reduced in comparison with the BLM group at Day 21. (C) The survival of mice from day 14 to day 21 in BLM, BLM+ADV, BLM+LPS and BLM+BLM groups were 100% (12/12), 66.7% (8/12), 50.0% (6/12) and 66.7% (8/12), respectively. *P<0.05, **P<0.01, ***P<0.001. AE, acute exacerbation; Ctrl, control; BLM, bleomycin; ADV, replication-defective adenoviral vectors; LPS, lipopolysaccharide.

Hydroxyproline content was measured using alkaline hydrolysis according to the manufacturer's instructions (cat. no. A030-2-1; Nanjing Jiancheng Bioengineering Institute). The absorbance was measured at 550 nm, and the hydroxyproline concentration in lung tissues was calculated using the formula provided in the kit instructions.

Histology and immunofluorescence. Paraffin-embedded lung tissue specimens were cut into 5-μm-thick sections. Sections were stained with H&E for histopathological evaluation. The severity of lung injury was assessed using a modified Ashcroft scale (32). All scoring was performed by three independent certified pathologists blinded to group allocation and the average score was used for analysis. Lung fibrosis was evaluated on sections stained with Masson's trichrome. For apoptosis detection, tissue sections were subjected to TUNEL staining according to the manufacturer's instructions (cat. no. KTA2011; Abbkine Scientific Co., Ltd.) and visualized using a fluorescence microscope (Thunder; Leica Microsystems GmbH). For immunofluorescence staining of alveolar epithelial cells, sections were incubated overnight at 4˚C with a pro-surfactant protein C (SPC) antibody (cat. no. ab211326; Abcam). Antigens were visualized using FITC-conjugated secondary antibodies (cat. no. 33112ES60; Shanghai Yeasen Biotechnology Co., Ltd.) incubated for 1 h at room temperature. Nuclei were counterstained with DAPI (cat. no. KGA215; Jiangsu KeyGen Biotech Co., Ltd.).

BALF cytospin and semi-quantitative cell analysis. BALF was centrifuged at 500 x g for 5 min at 4˚C. The cell pellet was resuspended in 200 μl of PBS. A 50 μl aliquot of the cell suspension was used for cytospin preparation. The slides were air-dried and stained with Giemsa stain (cat. no. C0131; Beyotime Biotechnology) according to the manufacturer's instructions. For each mouse, five representative microscopic fields (x400 magnification) were randomly selected and captured. In each field, the total number of nucleated cells was counted, and cells were classified into macrophages, lymphocytes and neutrophils based on standard morphological criteria: Macrophages by their large size, irregular nuclei and abundant cytoplasm; lymphocytes by their small size, round nuclei and scant cytoplasm; neutrophils by their segmented nuclei and pale pink cytoplasm. For each field, the relative proportion of each cell type was calculated as: Proportion of cell type=(number of that cell type in the field)/(total cells in the same field). These proportions are expressed as decimals (range 0-1). The data from the five fields per mouse were averaged for subsequent statistical analysis. Total cell count per mouse was defined as the average total nucleated cells per 400x field. All counting was performed by three independent investigators blinded to group allocation and the average values were used for analysis.

Micro-CT imaging and scoring. Chest radiological assessment was performed using a micro-CT system (Hiscan Micro CT; Suzhou Hiscan Information Technology Co., Ltd.). Image acquisition was standardized by positioning at three anatomical landmarks: The tracheal bifurcation, the level of the maximum cardiothoracic ratio and 1 mm above the diaphragmatic apex. Lung abnormalities were assessed using a modified Müller scoring system (33). At each of the three standardized levels, ground-glass opacities were scored on a 0-5 scale as follows: 0, no abnormality; 1, ≤5% affected area; 2, 5-25; 3, 25-50; 4, 50-75; 5, >75%. The scores from the three levels were averaged to obtain the mean micro-CT score

(range 0-5) for each animal. All scoring was performed by three independent investigators blinded to group allocation, and the average score was used for analysis.

ELISA. Serum and BALF supernatants were centrifuged at 1,500 x g for 5 min at 4˚C, and the pellets were discarded. Levels of IL-1β, IL-6 and TNF-α were determined using ELISA kits according to the manufacturer's instructions (cat. nos. MM-0040M1; MM-0163M1 and MM-0132M1; Jiangsu Enzyme Immunoassay Co., Ltd.). Absorbance was measured at 450 nm using a microplate reader and cytokine concentrations were calculated from standard curves.

Reverse transcription-quantitative PCR (RT-qPCR). Total RNA was extracted from lung tissues using TRIzol® reagent (Invitrogen; Thermo Fisher Scientific, Inc.) and reverse-transcribed into complementary DNA (cDNA) using the HiScript II Reverse Transcriptase kit (cat. no. R323-01; Vazyme Biotech Co., Ltd.). The thermocycling conditions for reverse transcription were as follows: 37˚C for 30 min and 85˚C for 5 sec. qPCR was performed using ChamQ Universal SYBR qPCR Master Mix (cat. no. Q711-02; Vazyme Biotech Co., Ltd.) on a QuantStudio 6 Flex Real-Time PCR System (Thermo Fisher Scientific, Inc.). The thermocycling conditions for qPCR were as follows: Initial denaturation at 95˚C for 20 sec, followed by 40 cycles of 95˚C for 10 sec and 60˚C for 30 sec, with a final melt curve analysis step to verify amplicon specificity. GAPDH was used as the internal reference gene, and its expression was confirmed to be stable across all experimental groups. Target gene mRNA levels were quantified using the comparative $2^{-\Delta\Delta Cq}$ method (34), with all samples normalized to the internal control GAPDH and calibrated to the average Ct value of the control group. Data were analyzed using QuantStudio™ Real-Time PCR Software (version 1.3; Thermo Fisher Scientific, Inc.). The primer sequences used for amplification are provided in Table SI.

Western blotting. Proteins were extracted from lung tissues using lysis buffer (cat. no. KGP2100; Jiangsu KeyGen Biotech Co., Ltd.). Protein concentration was determined using the bicinchoninic acid (BCA) method with a BCA protein assay kit (cat. no. P0012; Beyotime Biotechnology). Equal amounts of protein (10 μg per lane) were separated by SDS-PAGE using 12% gels, then transferred onto PVDF membranes. After blocking with Tris-buffered saline containing 0.1% Tween-20 (TBST) and 5% non-fat milk for 1 h at room temperature, the membranes were incubated with primary antibodies overnight at 4˚C. Subsequently, the membranes were incubated with HRP-conjugated secondary antibodies for 1 h at room temperature. The dilutions of all antibodies are provided in Table SII. Protein signals were visualized using a Tanon 5200 chemiluminescence imaging system. The antibodies used for western blotting are listed in Table SII.

Statistical analysis. All data are presented as mean ± SEM. Normality of distribution was assessed using the Shapiro-Wilk test (α=0.05) and visual inspection of Q-Q plots. For datasets meeting normality assumptions, comparisons between two groups were analyzed using an unpaired two-tailed Student's t-test, and comparisons among more than two groups were analyzed using one-way ANOVA followed by Dunnett's post hoc test for multiple comparisons (comparing each AE group to the BLM-only control). For data not meeting normality assumptions, the Kruskal-Wallis test with Dunn's post hoc correction was used. Outliers were identified using Grubbs' test (α=0.05) and confirmed by reviewing experimental records. No outliers were excluded from the final analysis. Post hoc power analysis was performed to confirm that the sample sizes were adequate to detect meaningful differences (power >0.99 for the primary outcome measure). $P<0.05$ was considered to indicate a statistically significant difference. Exact P-values are reported for $P\geq0.01$, while $P<0.01$ and $P<0.001$ are indicated as such. The western blotting images were analyzed by ImageJ software (National Institutes of Health). Statistical analyses were performed by GraphPad Prism version 8 (Dotmatics).

Results

Weights and survival of AE-PF mice. Mice in the BLM group exhibited a gradual decrease in body weight compared with the control group. Following intratracheal rechallenge with ADV, LPS or a second dose of BLM on day 14 after the initial BLM treatment, mice in all three AE groups showed more pronounced weight loss and lower survival rates when compared with mice receiving a single dose of BLM (Fig. 1B and C).

On day 21, the mean body weights of the ADV group (17.41±1.59 g; n=8), LPS group (16.52±0.61 g; n=6) and two-dose BLM group (16.83±1.30 g; n=8) were significantly reduced compared with that of the single-dose BLM group (20.96±2.23 g; n=12; all $P<0.01$; Fig. 1B).

Following administration of the AE-inducing agents, the survival rate of the BLM+LPS group (50.0%) was significantly lower when compared with that of the BLM group (100%; $P=0.019$). Although the survival rates of the BLM+ADV group (66.7%) and the BLM+BLM group (66.7%) were lower when compared with that of the BLM group, the differences did not reach statistical significance. No significant differences in survival rates were observed among the three AE subgroups (Fig. 1C).

Chest Micro-CT and lung histopathology of AE-PF mouse models. Micro-CT scans were performed on day 20 in BLM-treated mice. Compared with the BLM group, mice in all three AE groups exhibited larger areas of ground-glass opacities in the lungs. According to the modified Müller scoring criteria (33), the mean CT lesion scores in the BLM+ADV (4.67±0.41), BLM+LPS (4.56±0.19) and BLM+BLM (4.20±0.30) groups were significantly higher when compared with those in the BLM group (2.78±0.84; all $P<0.01$). No significant differences were observed among the three AE subgroups (Fig. 2A and B).

Gross lung tissue specimens from the Ctrl group exhibited normal morphology, soft texture and no congestion or edema. By contrast, lungs from the BLM group showed focal injury characterized by congestion, edema and consolidation. Importantly, lung injury was more severe in all three AE groups, as evidenced by larger lesional areas and, in some cases, complete lung consolidation (Fig. 2C). Histopathological examination of lung tissues with H&E staining revealed

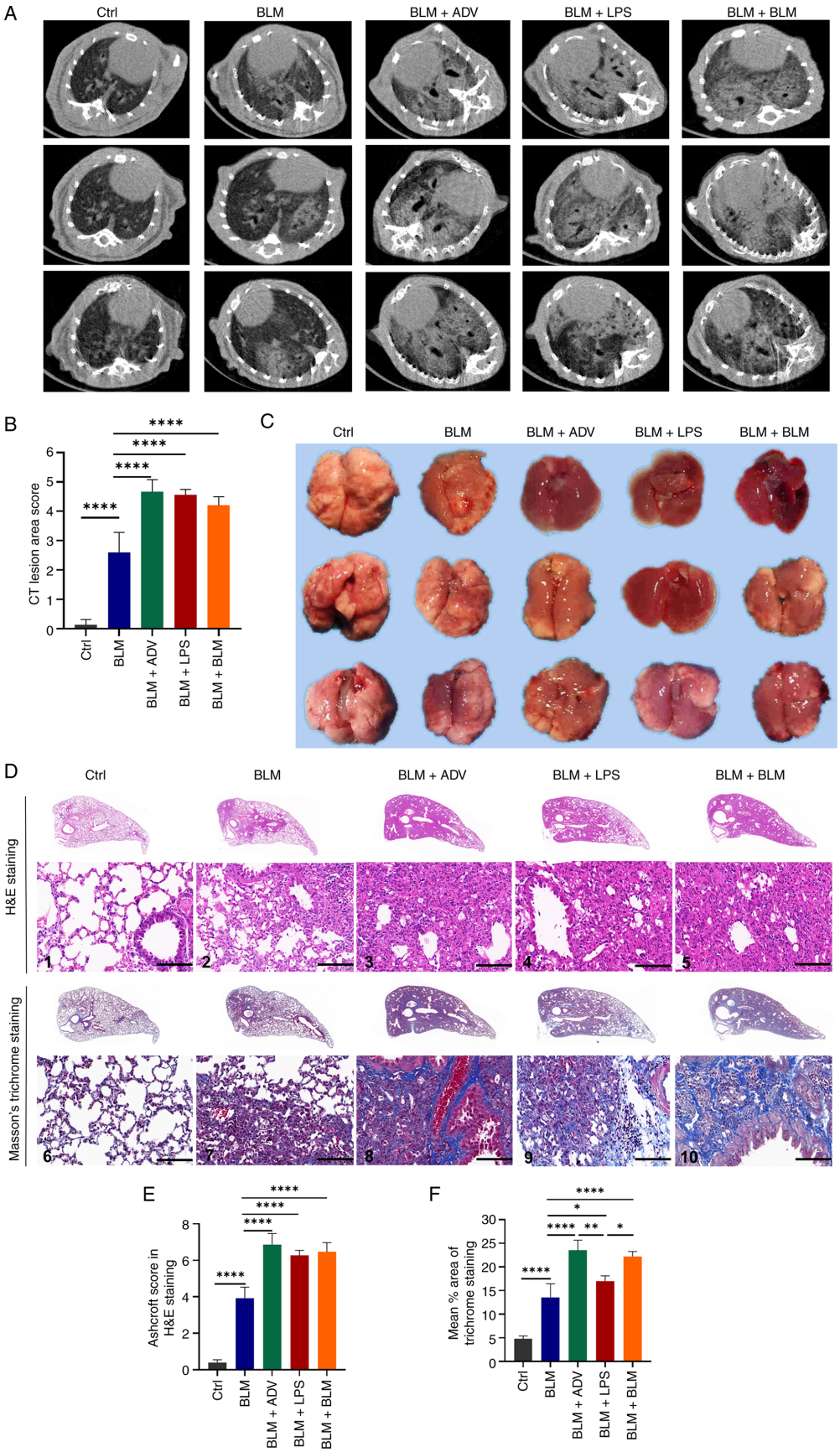

Figure 2. The chest imaging and pathology in AE-PF mouse models by intratracheally instillation with ADV, LPS and a second dose of BLM. (A) Chest micro-CT scans showed the lung injury area. (B) Modified Müller scoring system (33) CT lesion area scores (n=6). (C) Gross lung tissue specimens showed that the severity of lung injury was more exacerbated in three AE groups compared with BLM group. (D) H&E and Masson's trichrome staining of lung tissues indicated that the AE groups exhibited significantly more severe lung injury and fibrosis compared with the BLM group. (E) Ashcroft score of lung tissues in HE or Masson staining on day 21 (each group, n=6). (F) Quantification of blue-stained area percentage of lung tissues in Masson's trichrome staining (each group, n=6). *P<0.05, **P<0.01 and ****P<0.0001. Scale bar, 100 μm. AE, acute exacerbation; CT, computer tomography; Ctrl, control; BLM, bleomycin; ADV, adenoviral vectors; LPS, lipopolysaccharide.

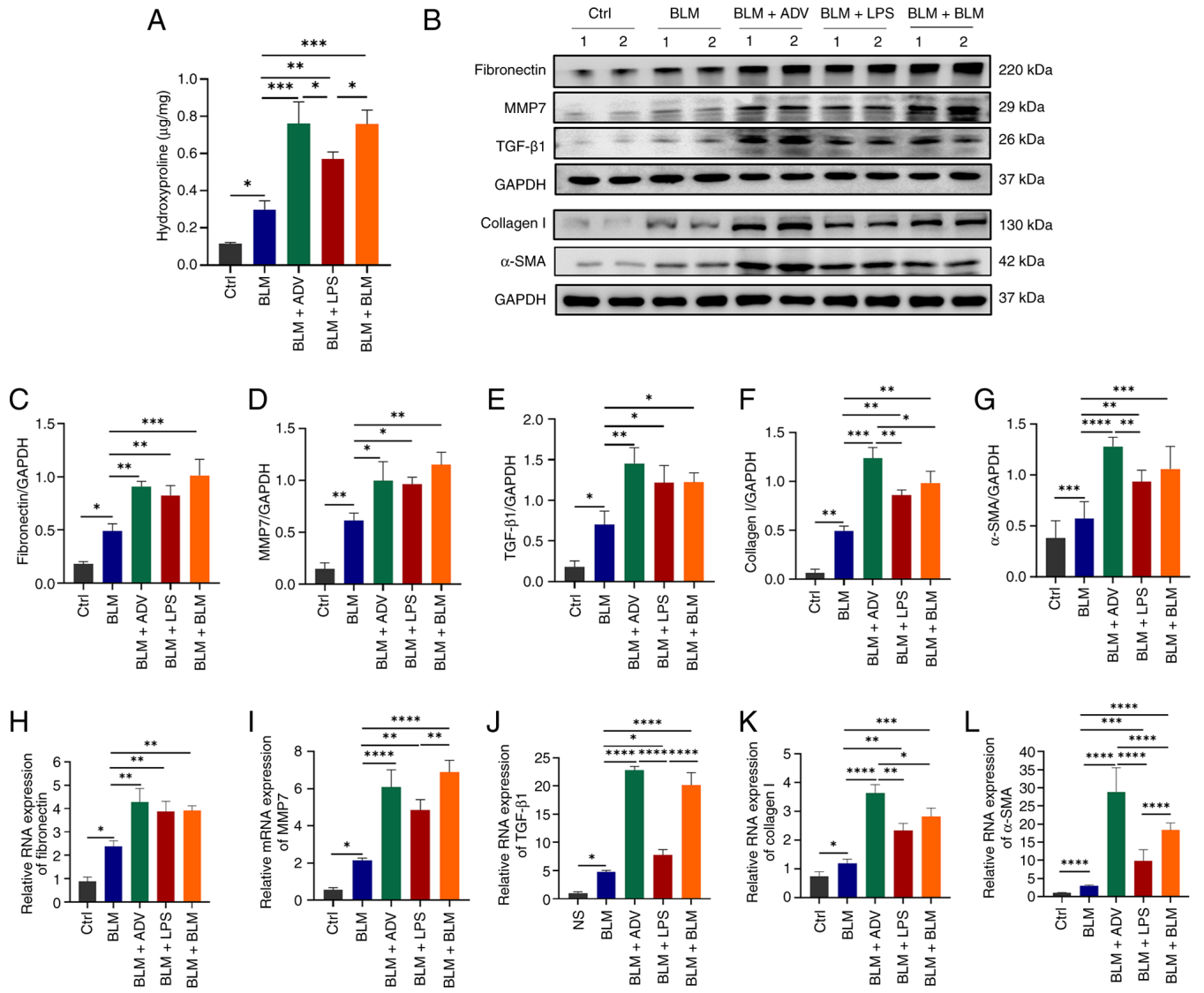

Figure 3. The pulmonary fibrosis of three AE group mice was significantly aggravated compared with the BLM group. (A) The hydroxyproline contents in both BLM+ADV and BLM+BLM groups of mice were higher than in the BLM+LPS group animals (each group, n=6). (B) Western blotting analysis revealed that the expressions of fibrosis markers Fibronectin, MMP-7, TGF-β1, Collagen I and α-SMA in the AE groups were significantly upregulated compared with the BLM group. (C) Semi-quantification of Fibronectin protein expression relative to GAPDH. (D) Semi-quantification of MMP-7 protein expression relative to GAPDH. (E) Semi-quantification of TGF-β1 protein expression relative to GAPDH. (F) Semi-quantification of Collagen I protein expression relative to GAPDH. (G) Semi-quantification of α-SMA protein expression relative to GAPDH (each group, n=6). The relative mRNA expressions of fibrosis markers (H) Fibronectin, (I) MMP-7, (J) TGF-β1, (K) Collagen I and (L) α-SMA in the AE groups were significantly increased compared with the BLM group by qPCR (each group, n=6). *P<0.05, **P<0.01, ***P<0.001, ****P<0.0001. Scale bar, 50 μm. AE, acute exacerbation; BLM, bleomycin; ADV, adenoviral vectors; LPS, lipopolysaccharide; α-SMA: α-smooth muscle actin.

alveolar septal congestion and edema, excessive inflammatory cell infiltration and alveolar epithelial cell damage in AE mice. In comparison, the BLM group showed less inflammatory cell infiltration and a smaller extent of damage (Fig. 2D). The modified Ashcroft scores (32) in the BLM+ADV (6.87±0.61), BLM+LPS (6.27±0.28) and BLM+BLM (6.47±0.51) groups were significantly higher when compared with those in the single-dose BLM group (3.93±0.60; all P<0.0001). No significant differences were observed among the three AE subgroups (Fig. 2E).

Masson's trichrome staining showed mild collagen deposition around the trachea or blood vessels in the control group and more extensive deposition in the single-dose BLM group. Compared with both control and single-dose BLM groups, all three AE groups exhibited markedly increased collagen deposition surrounding the bronchi, within the alveolar septa and in remodeled lung regions (Fig. 2D). Quantitative analysis revealed that the proportion of Masson's staining area was significantly higher in each AE group when compared with in the single-dose BLM group (P<0.0001 for ADV and two-dose BLM groups; P=0.017 for LPS group). Furthermore, among the AE subgroups, both the BLM+ADV and BLM+BLM groups had significantly higher scores when compared with the BLM+LPS group (P<0.01 and P=0.011, respectively; Fig. 2F).

The expressions of fibrotic markers are significantly upregulated in the lungs of AE-PF mouse models. The present study observed a significant increase in total collagen content, as

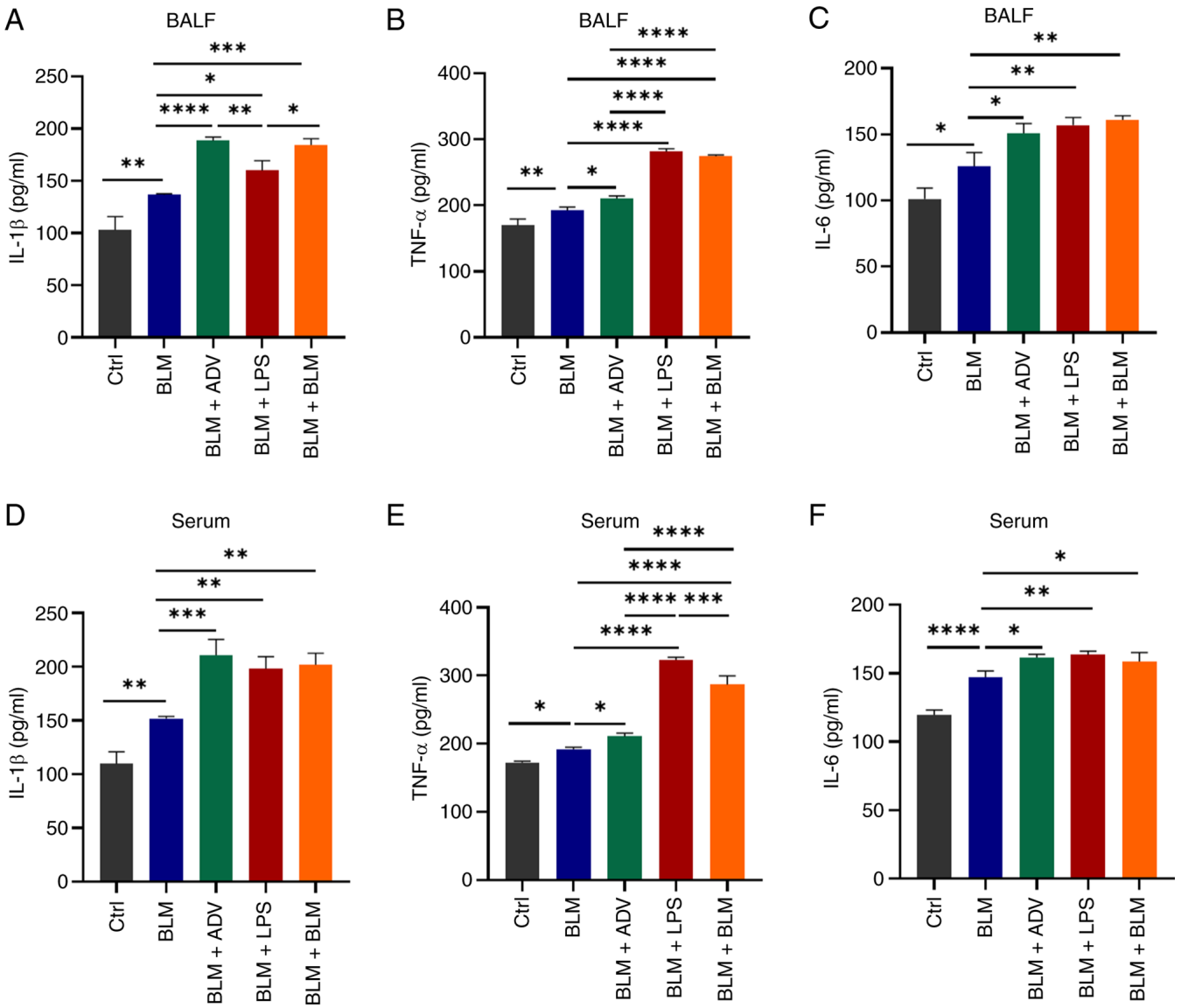

Figure 4. The levels of inflammatory cytokines in BALF and serum were significantly elevated in AE-PF mice by ELISA. The levels of (A) IL-1β, (B) TNF-α and (C) IL-6 in BALF were significantly elevated in three AE-PF group mice compared with BLM group. The findings of the BLM group were significantly increased when compared with the Ctrl group (each group, n=6). The levels of (D) IL-1β, (E) TNF-α and (F) IL-6 in serum were significantly elevated in three AE-PF groups of mice compared with BLM group. The findings of the BLM group were significantly increased when compared with the Ctrl group (each group, n=6). *P<0.05, **P<0.01, ***P<0.001, ****P<0.0001. AE, acute exacerbation; BALF, bronchoalveolar lavage fluid; Ctrl, control; BLM, bleomycin; ADV, adenoviral vectors; LPS, lipopolysaccharide.

determined by hydroxyproline assay, in the BLM+ADV group (0.75±0.09 μg/mg), BLM+LPS group (0.59±0.07 μg/mg) and BLM+BLM group (0.77±0.06 μg/mg) compared with the single-dose BLM group (0.29±0.04 μg/mg; P<0.001; P<0.01 and P<0.001, respectively). The BLM+ADV and BLM+BLM groups showed significantly higher hydroxyproline levels when compared with the BLM+LPS group (P=0.041 and P=0.044, respectively; Fig. 3A).

Similarly, western blotting revealed that the expression levels of the profibrotic markers fibronectin, MMP7, TGF-β1, collagen I and α-smooth muscle action (α-SMA) were significantly upregulated in all three AE subgroups compared with the single-dose BLM group. Collagen I expression in the lungs of the BLM+ADV group was significantly higher when compared with that in the BLM+LPS group (P<0.01) and the BLM+BLM group (P=0.026), respectively. Likewise, α-SMA protein expression in lung tissue was significantly higher in the BLM+ADV group when compared with that in the BLM+LPS group (P<0.01). No significant differences in other indices were observed among the three AE-PF subgroups (Fig. 3B-G).

RT-qPCR showed that the mRNA expression levels of fibronectin, MMP7, TGF-β1, collagen I and α-SMA were significantly increased in the BLM group compared with the control group. All three AE groups had significantly higher mRNA levels of these markers when compared with the BLM group. No significant differences in fibronectin mRNA levels were detected among the three AE subgroups. The mRNA level of MMP7 was significantly higher in the BLM+BLM group when compared with that in the BLM+LPS group (P<0.01). The mRNA levels of TGF-β1 were significantly higher in the BLM+ADV group (P<0.0001) and the BLM+BLM group (P<0.0001) compared with the BLM+LPS group. Collagen

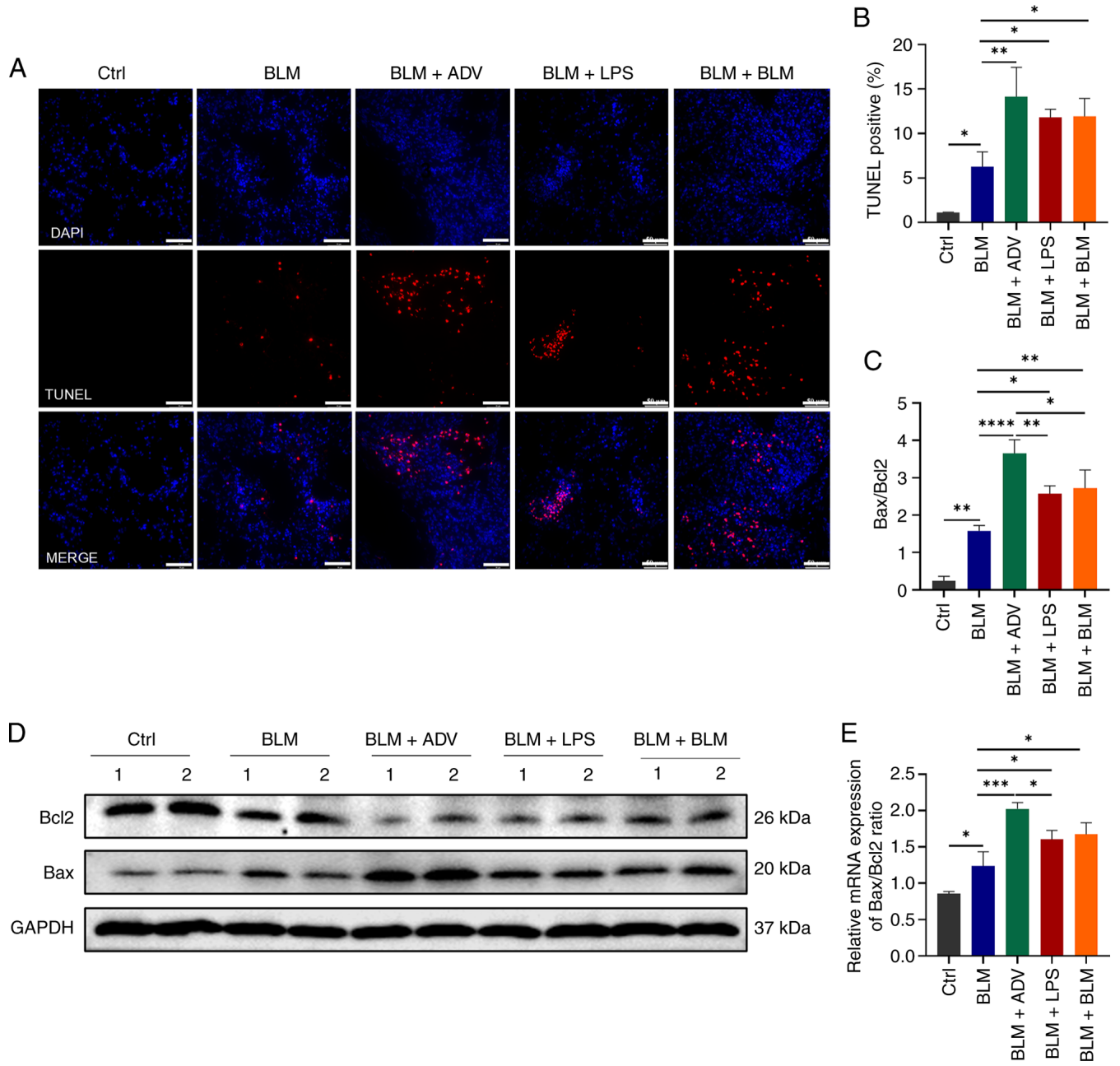

Figure 5. Apoptosis was significantly enhanced in AE-PF mice, particularly in the BLM+ADV group. (A) Representative TUNEL staining images of lung tissues from each group. (B) Quantification of TUNEL-positive cells showed that the percentages in the AE groups were significantly higher than in the BLM group, particularly in the BLM+ADV group (each group, n=6). (C) Quantification of the Bax/Bcl2 ratio revealed a significant increase in the BLM+ADV group compared with both the BLM+LPS and BLM+BLM groups (each group, n=6). (D) Representative western blotting bands showing the protein expression of Bcl2 and Bax in each group. (E) The findings of quantitative-PCR analysis showed the Bax/Bcl2 ratio was significantly enhanced in three AE-PF group mice when compared with BLM group (each group, n=6). *P<0.05, **P<0.01, ***P<0.001, ****P<0.0001. Scale bar: 50 μm. AE, acute exacerbation; BLM, bleomycin; ADV, adenoviral vectors; LPS, lipopolysaccharide.

I mRNA levels in the BLM+ADV group were significantly higher when compared with those in the BLM+LPS group (P<0.01) and the BLM+BLM group (P=0.019). The mRNA level of α-SMA in the BLM+ADV group was significantly higher when compared with that in both the BLM+BLM and BLM+LPS groups (both P<0.0001; Fig. 3H-L).

Excessive inflammation is observed in AE-PF mice models. Analysis of inflammatory cytokine levels in BALF and serum by ELISA showed that IL-1β, TNF-α and IL-6 were significantly elevated in the BLM group compared with the control group, but remained significantly lower when compared with those in the three AE groups. When comparing cytokine levels among the three AE subgroups, BALF IL-1β levels were significantly higher in the BLM+ADV and BLM+BLM groups than in the BLM+LPS group (P<0.01 and P=0.021, respectively), whereas no significant differences were observed in serum IL-1β levels (Fig. 4A and D). TNF-α levels in both BALF and serum were significantly higher in the BLM+LPS and BLM+BLM groups compared with the BLM+ADV group (all P<0.0001; Fig. 4B and E). Furthermore, serum TNF-α levels in the BLM+LPS group were significantly higher when

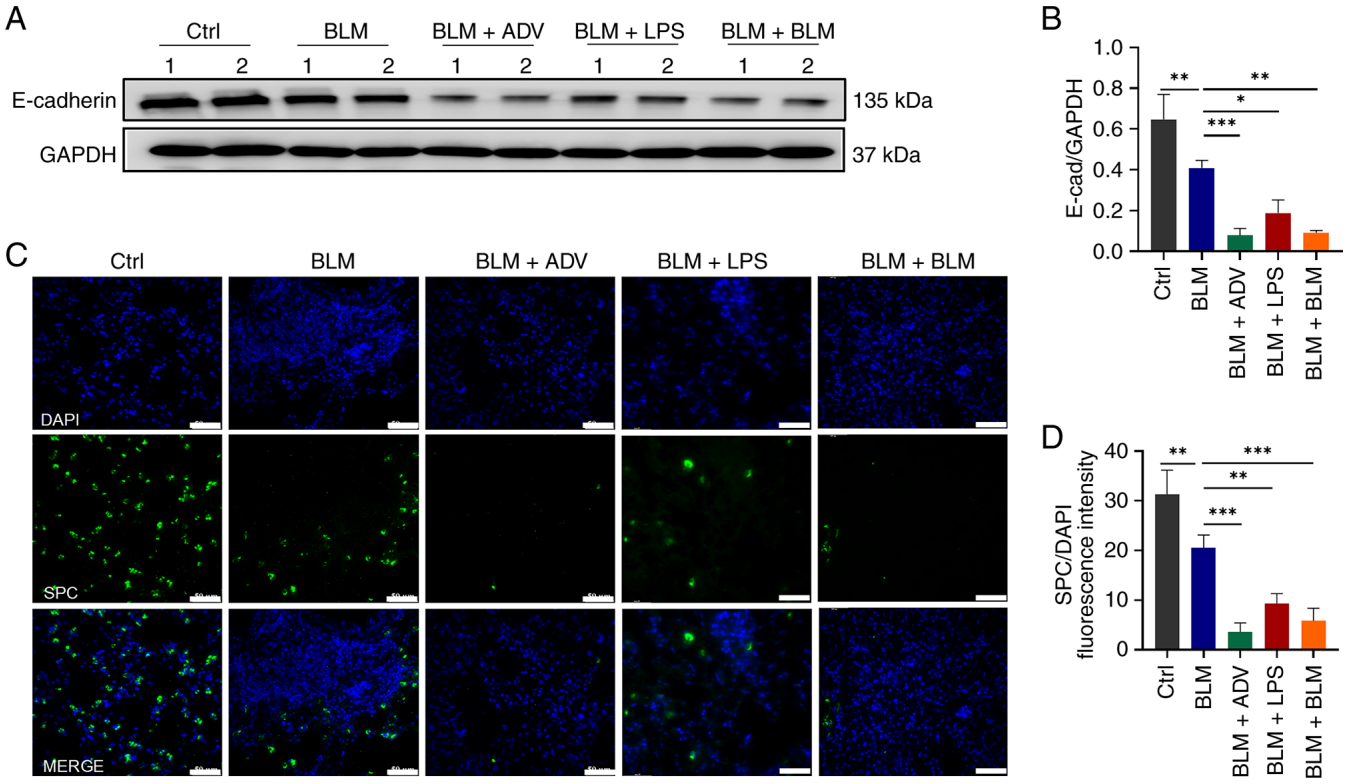

Figure 6. Epithelial cell injury was significantly enhanced in the AE-PF mice. (A) Western blotting analysis of E-cadherin protein expression. (B) Quantification of E-cadherin expression relative to GAPDH (each group, n=6). (C) Representative immunofluorescence images of SPC staining. (D) Quantification of SPC fluorescence intensity (each group, n=6). *P<0.05, **P<0.01, ***P<0.001. Scale bar, 50 μm. AE, acute exacerbation; BLM, bleomycin; ADV, adenoviral vectors; LPS, lipopolysaccharide; SPC, pro-surfactant protein C.

compared with those in the two-dose BLM group (P<0.001; Fig. 4E). No significant differences in IL-6 levels were observed among the AE subgroups in either BALF or serum (Fig. 4C and F).

Giemsa staining of BALF cytospin preparations revealed distinct cellular compositions across the groups (Fig. S1). Compared with the control group, the total cell count was significantly increased in the BLM group, and further elevated in all three AE groups. The proportion of lymphocytes was significantly higher in the BLM+ADV group when compared with that in the BLM+LPS and BLM+BLM groups. The percentages of macrophages in the BLM+LPS and BLM+BLM groups were significantly higher when compared with those in the BLM+ADV group. The proportion of neutrophils in the BLM+LPS group was significantly greater when compared with that in the BLM+ADV and BLM+BLM groups.

Apoptosis is increased in lung tissues of AE-PF mice. The enhanced apoptosis of alveolar epithelial cells plays a key role in the pathogenesis of AE-IPF (35). The present study therefore investigated apoptosis in lung tissues of the mouse models. TUNEL assays revealed no clear positive signals in the control group. The percentage of TUNEL-positive cells in the BLM group was significantly higher when compared with that in the control group (P=0.049). Conspicuous and aggregated apoptotic signals were observed in lung tissues of all three AE groups. Notably, mice in the BLM+ADV, BLM+LPS and BLM+BLM groups exhibited significantly increased apoptosis compared with the BLM group (P<0.01; P=0.035 and P=0.032, respectively) (Fig. 5A and B). No statistically significant differences were observed among the three AE subgroups, although the BLM+ADV subgroup showed a trend toward higher values.

The present study further analyzed the protein and mRNA expression of apoptosis-related molecules in the AE-PF mouse models. In the BLM group, the pro-apoptotic molecule Bax was significantly increased compared with the control group, but its level was significantly lower when compared with that in the three AE groups (Fig. 5D). By contrast, the expression level of the anti-apoptotic factor Bcl2 was significantly reduced in the BLM group compared with the control group, and the AE groups showed a further decrease relative to the BLM group (Fig. 5D). The Bax/Bcl2 ratio, reflecting apoptotic propensity, was highest in the BLM+ADV group among the three AE subgroups. This group exhibited significantly higher Bax/Bcl2 ratios when compared with the BLM+LPS group (P<0.01) and the BLM+BLM group (P=0.022; Fig. 5C). qPCR analysis also demonstrated that the Bax/Bcl2 ratio was significantly higher in the BLM+ADV group compared with that in the BLM+LPS group (P=0.020; Fig. 5E).

The expression of AEC2 markers is significantly downregulated, suggesting that the damage to AEC2 is aggravated in the lung of AE-PF mice. Western blotting analysis demonstrated a significant decrease in E-cadherin expression in all three AE groups compared with the single-dose BLM group (Fig. 6A and B). The present study also analyzed the expression of the AEC2 marker SPC in lung tissues. SPC expression

was significantly reduced in the BLM group and further decreased in mice from the AE groups, indicating that AEC2s were substantially damaged following the induction of acute exacerbation (Fig. 6C and D).

Discussion

The pathogenesis of AE-IPF remains unclear, and it is uncertain whether acute exacerbations represent an inherent acceleration of the underlying fibrotic disease or a reaction to external, often unidentified triggers that lead to acute respiratory distress syndrome (ARDS) (36). Existing studies have identified viral, bacterial and toxic injuries as contributors to AE-IPF (10,17,37,38). The underlying mechanisms may include increased apoptosis of AEC2s, excessive lung inflammation and extracellular matrix deposition (17). Pathologically, AE-IPF often presents as new diffuse alveolar damage, occasionally accompanied by hyaline membrane formation, superimposed on a background of usual interstitial pneumonia (2). Multiple animal models of AE-PF induced by viruses, bacteria, drugs or surgery have been reported (19,23,26,28,29). However, each model possesses inherent limitations, including suboptimal timing for AE induction, imperfect experimental methods, prolonged experimental design cycles or an oversimplified assumption that AE is solely caused by external insults, thereby overlooking potential contributions from the disease process itself (17). Consequently, there is an urgent need to systematically compare and analyze these different animal models to identify a more robust and clinically relevant platform, thereby laying the groundwork for subsequent preclinical research.

The conventional animal model for studying pulmonary fibrosis is established by intratracheal instillation of a single dose of BLM, which has proven instrumental in elucidating the mechanisms underlying alveolar epithelial cell injury and subsequent fibrosis progression (17,39). Therefore, the present study developed AE-PF mouse models based on BLM-induced pulmonary fibrosis using three distinct triggers: ADV, LPS and a second dose of BLM. Analysis demonstrated that all three triggers effectively induced clinical, imaging and histopathological exacerbations in the lungs, accompanied by molecular marker changes in inflammation, apoptosis and fibrosis that recapitulate features observed in AE-IPF. However, the degrees of apoptosis, pulmonary fibrosis and inflammatory response in lung tissue differed among the three AE-PF models. Compared with the BLM+LPS group, BLM+ADV mice exhibited more pronounced apoptosis and lung fibrosis but lower TNF-α levels in both BALF and serum. Compared with mice receiving two doses of BLM, those treated with ADV in combination with BLM showed significantly higher levels of apoptosis, collagen I and α-SMA mRNA, while TNF-α levels in both BALF and serum were significantly lower. Compared with the BLM+LPS group, the two-dose BLM group exhibited more severe lung fibrosis, with similar levels of lung apoptosis and BALF TNF-α. The causes and mechanisms underlying the differences among these three AE-PF models warrant further investigation.

Adenovirus is highly contagious and often leads to outbreaks of respiratory infection in closed or crowded environments (40). Weng *et al* (37) analyzed serum samples from 41 patients with AE-IPF and 108 patients with stable IPF, reporting that 7.3% of AE-IPF patients tested positive for adenovirus-specific IgM antibodies, compared with only 0.9% of stable patients with IPF (37). Latent adenovirus can persist in lymphoid or other tissues for extended periods, with the possibility of reactivation in severely immunosuppressed patients (41). In light of this, the present study used replication-deficient ADV, which retains immunogenicity but lacks replicative capacity, to induce AE-PF in BLM-treated mice. To the best of our knowledge, this approach has not been reported previously.

The mechanisms by which ADV infection exacerbates pulmonary fibrosis may involve two interrelated pathways (17,42). First, ADV itself may directly damage the lung parenchyma, potentially triggering aberrant wound healing responses that lead to AE-PF. Second, ADV infection activates the immune system, recruiting macrophages and Th2 cells to the site of injury. These cells release large amounts of pro-inflammatory and pro-fibrotic factors, including TGF-β, TNF-α, IL-1 and IL-6, through signaling pathways such as the TNF-α/NF-κB pathway, the IL-6/STAT pathway and the TGF-β/SMAD pathway, ultimately contributing to the pathogenesis of AE-PF.

LPS is commonly used in various preclinical models to induce conditions such as ARDS or peritoneal inflammation (43-46). Given the pathological features of ARDS observed in lung tissue from patients with AE-IPF, Kimura *et al* (28) established a mouse model of AE-PF by administering BLM followed by LPS. However, they collected specimens on day 1 after LPS treatment (day 8 after BLM treatment), a stage when lung inflammation is most pronounced but fibrosis remains relatively mild (28). Guo *et al* (47) induced an AE-PF model in BLM-treated mice using LPS on day 14 and assessed the effects on day 15, reporting no significant progression of pulmonary fibrosis (47). By contrast, in the present AE-PF model, LPS was administered on day 14 after BLM treatment, during the stage of established lung fibrosis, and lung samples were collected on day 21. Administering triggering agents and collecting samples at appropriate time points in BLM-treated mice will help improve researchers' understanding of the pathophysiological processes and explore the pathogenesis of AE-IPF.

A systematic review and meta-analysis revealed that patients with AE-IPF with elevated neutrophil counts in BALF have a high risk of mortality (48). A previous study showed that germ-free BLM-treated mice exhibit a similar degree of lung injury compared with wild-type BLM-treated mice; however, germ-free mice are protected from mortality (38). Another single-center retrospective study of patients with IPF reported that among seven patients with bacterial infections, one developed AE-IPF and two died during a 60-month follow-up period. Among 12 patients with viral infections, one developed AE-IPF, but no mortalities occurred (49). These findings may explain why, among the three AE-PF models, the mortality rate was highest in the BLM+LPS group. This is likely attributable to the inflammatory response associated with bacterial infection and LPS, which can lead to a high mortality rate.

To elucidate the molecular mechanisms underlying acute exacerbations induced by 'idiopathic' AE or non-infectious factors, previous studies have demonstrated that administering BLM two or more times can successfully establish mouse models of AE-PF (29,50,51). The two-dose BLM model has

been established by administration on days 0 and 21, with outcome assessment on day 35. The multiple-dose model has been administered once every 2 weeks for a total of six doses. However, the duration of these studies is excessively long, ranging from 5 to 12 weeks. The present findings demonstrated that administering the same dose of BLM on day 14 after the initial dose yielded model outcomes assessed on day 21 that closely resembled those of the long-cycle mouse model. These manifestations included significantly increased lung fibrosis and apoptosis, along with elevated levels of inflammatory cytokines such as TNF-α, IL-6 and IL-1β. Accordingly, the present study successfully induced AE-PF in mice using this two-dose BLM administration regimen. Thus, this approach offers a stable, reliable, short-duration and reproducible method for establishing an animal model of non-infectious AE-PF, thereby providing a valuable tool for future research.

Among the three AE models evaluated in the present study, the ADV-triggered BLM model most comprehensively recapitulated the key pathological features of human AE-IPF. First, the BLM+ADV group exhibited the most severe fibrotic phenotype, as reflected by the highest levels of collagen I, α-SMA and TGF-β, as well as the highest fibrosis scores on histological assessment. Although hydroxyproline content was slightly lower than that in the BLM+BLM group, this discrepancy may reflect differences in collagen turnover or maturation, as hydroxyproline measures total collagen content, whereas collagen I and α-SMA reflect active fibrogenesis. Collectively, these findings indicate a robust and active fibrotic response in the BLM+ADV model. Second, this group also exhibited the most pronounced alveolar epithelial apoptosis, which is recognized as a key driver of AE-IPF pathogenesis. Alveolar epithelial injury is considered to trigger aberrant wound healing and fibroblast activation, contributing to the rapid decline in lung function. Third, the ADV group displayed a moderate yet significant increase in cytokines (Table SIII). Previous studies have reported elevated levels of multiple cytokines in patients with AE-IPF, including IL-1β, TNF-α and IL-6 (52-55), findings that are well aligned with the pathological features of human AE-IPF. Human AE-IPF is characterized by a complex interplay of fibrosis, epithelial injury and inflammation. Collectively, these findings suggest that the ADV-triggered BLM model provides a translational platform that captures the core pathological features of AE-IPF, including robust fibrogenesis (elevated collagen I, α-SMA, TGF-β and fibrosis scores), prominent epithelial apoptosis and a moderate inflammatory response. This model may therefore be particularly suitable for studying the mechanisms underlying acute exacerbations and for evaluating targeted therapeutic interventions.

The present study has some limitations. The mortality rates observed in the AE models (33.3-50%) are consistent with the high mortality reported in patients with AE-IPF (56-100%) (5), supporting the translational relevance of these models. While this high mortality is clinically reflective, it should be considered as a practical consideration for future preclinical studies. Although the bleomycin-induced fibrosis model recapitulates key histopathological features of human IPF, it does not fully replicate the chronic, progressive nature of the disease. Moreover, species differences in immune response and lung anatomy, as well as the short observation period (21 days), may limit the translation of the AE phenotype to the long-term human disease course. In clinical practice, new ground-glass opacities and/or consolidations superimposed on pre-existing pulmonary fibrosis are typically observed on chest imaging in patients with AE-IPF. However, the present study only compared chest CT changes between AE-PF mice and BLM-treated animals at a single time point, without longitudinal tracking of the same animals before and after the second challenge. The present study acknowledges that incorporating serial chest CT imaging and longitudinal BALF cytological classification in the same mice would better facilitate understanding of the progression and evolution of pulmonary fibrosis. Although the sample sizes (n=6-8 per group) were sufficient to detect statistically significant differences, as confirmed by post hoc power analysis, they remain relatively modest. Future studies with larger cohorts may help further validate these findings and allow for more detailed subgroup analyses. The mechanisms underlying acute exacerbation in mouse models of pulmonary fibrosis require further investigation.

The present study demonstrated that three triggers, ADV, LPS and a second dose of BLM, effectively induce AE-PF in BLM-treated mice by promoting enhanced apoptosis, excessive inflammation and fibrosis progression. Although the severity of apoptosis, inflammation and lung fibrosis progression differed among the three AE-PF models, the protocol of rechallenging mice on day 14 after conventional BLM treatment may serve as a standardized AE-PF model. In comparison, the ADV-induced BLM mouse model may represent a superior platform for studying AE-PF.

Acknowledgements

Not applicable.

Funding

This work was supported by National Natural Science Foundation of China (grant nos. 82570105, 82070064, 81670059 and 81200049). and Fundings for Clinical Trials from the Affiliated Drum Tower Hospital, Medical School of Nanjing University (grant no. 2022-LCYJ-MS-11).

Availability of data and materials

The data generated in the present study may be requested from the corresponding author.

Authors' contributions

XuY and MZ were responsible for the experiments and drafting the manuscript. ML, HZ and QL analyzed the images of histopathology and supplemented experiments. XiY contributed to the experimental design, performed the experiments, acquired and analyzed the primary data, and prepared the figures. CJ participated in data analysis and interpretation, and prepared the figures. XH contributed to the study conception, supervised the experiments and critically reviewed and revised the draft. MC designed the study and reviewed and approved the final manuscript. XuY and MC confirm the authenticity of all the raw data. All authors have read and approved the final manuscript.

Ethics approval and consent to participate

The present study was approved by the Ethics Committee of Nanjing Drum Tower Hospital, Nanjing University Medical School (Nanjing, China; approval no. 2016-160-01).

Patient consent for publication

Not applicable.

Competing interests

The authors declare that they have no competing interests.

References

1. Raghu G, Remy-Jardin M, Richeldi L, Thomson CC, Inoue Y, Johkoh T, Kreuter M, Lynch DA, Maher TM, Martinez FJ, *et al*: Idiopathic pulmonary fibrosis (an update) and progressive pulmonary fibrosis in adults: An official ATS/ERS/JRS/ALAT clinical practice guideline. Am J Respir Crit Care Med 205: e18-e47, 2022.
2. Raghu G, Remy-Jardin M, Myers JL, Richeldi L, Ryerson CJ, Lederer DJ, Behr J, Cottin V, Danoff SK, Morell F, *et al*: Diagnosis of idiopathic pulmonary fibrosis. An official ATS/ERS/JRS/ALAT clinical practice guideline. Am J Respir Crit Care Med 198: e44-e68, 2018.
3. Naccache JM, Jouneau S, Didier M, Borie R, Cachanado M, Bourdin A, Reynaud-Gaubert M, Bonniaud P, Israël-Biet D, Prévot G, *et al*: Cyclophosphamide added to glucocorticoids in acute exacerbation of idiopathic pulmonary fibrosis (EXAFIP): A randomised, double-blind, placebo-controlled, phase 3 trial. Lancet Respir Med 10: 26-34, 2022.
4. Fabbrizzi A, Nannini G, Lavorini F, Tomassetti S and Amedei A: Microbiota and IPF: Hidden and detected relationships. Sarcoidosis Vasc Diffuse Lung Dis 38: e2021028, 2021.
5. Marchioni A, Tonelli R, Ball L, Fantini R, Castaniere I, Cerri S, Luppi F, Malerba M, Pelosi P and Clini E: Acute exacerbation of idiopathic pulmonary fibrosis: Lessons learned from acute respiratory distress syndrome? Crit Care 22: 80, 2018.
6. Juarez MM, Chan AL, Norris AG, Morrissey BM and Albertson TE: Acute exacerbation of idiopathic pulmonary fibrosis-a review of current and novel pharmacotherapies. J Thorac Dis 7: 499-519, 2015.
7. Jenkins RG, Moore BB, Chambers RC, Eickelberg O, Königshoff M, Kolb M, Laurent GJ, Nanthakumar CB, Olman MA, Pardo A, *et al*: An official american thoracic society workshop report: Use of animal models for the preclinical assessment of potential therapies for pulmonary fibrosis. Am J Respir Cell Mol Biol 56: 667-679, 2017.
8. Khor YH: Antifibrotic therapy for idiopathic pulmonary fibrosis: Combining real world and clinical trials for totality of evidence. Chest 160: 1589-1591, 2021.
9. Kreuter M and Maher TM: Treatment of acute exacerbation of idiopathic pulmonary fibrosis. A call to arms. Am J Respir Crit Care Med 201: 1030-1032, 2020.
10. Collard HR, Ryerson CJ, Corte TJ, Jenkins G, Kondoh Y, Lederer DJ, Lee JS, Maher TM, Wells AU, Antoniou KM, *et al*: Acute exacerbation of idiopathic pulmonary fibrosis. An international working group report. Am J Respir Crit Care Med 194: 265-275, 2016.
11. Kreuter M, Polke M, Walsh SLF, Krisam J, Collard HR, Chaudhuri N, Avdeev S, Behr J, Calligaro G, Corte T, *et al*: Acute exacerbation of idiopathic pulmonary fibrosis: International survey and call for harmonisation. Eur Respir J 55: 1901760, 2020.
12. McElroy AN, Invernizzi R, Laskowska JW, O'Neill A, Doroudian M, Moghoofei M, Mostafaei S, Li F, Przybylski AA, O'Dwyer DN, *et al*: Candidate role for Toll-like receptor 3 L412F polymorphism and infection in acute exacerbation of idiopathic pulmonary fibrosis. Am J Respir Crit Care Med 205: 550-562, 2022.
13. Molyneaux PL, Cox MJ, Wells AU, Kim HC, Ji W, Cookson WO, Moffatt MF, Kim DS and Maher TM: Changes in the respiratory microbiome during acute exacerbations of idiopathic pulmonary fibrosis. Respir Res 18: 29, 2017.
14. Stoolman JS, Vannella KM, Coomes SM, Wilke CA, Sisson TH, Toews GB and Moore BB: Latent infection by γherpesvirus stimulates profibrotic mediator release from multiple cell types. Am J Physiol Lung Cell Mol Physiol 300: L274-L285, 2011.
15. Ghincea A, Ryu C and Herzog EL: An acute exacerbation of idiopathic pulmonary fibrosis after BNT162b2 mRNA COVID-19 vaccination: A case report. Chest 161: e71-e73, 2022.
16. Bando T, Takei R, Mutoh Y, Sasano H, Yamano Y, Yokoyama T, Matsuda T, Kataoka K, Kimura T and Kondoh Y: Acute exacerbation of idiopathic pulmonary fibrosis after SARS-CoV-2 vaccination. Eur Respir J 59: 2102806, 2022.
17. Ye X, Zhang M, Gu H, Liu M, Zhao Y, Shi Y, Wu S, Jiang C, Ye X, Zhu H, *et al*: Animal models of acute exacerbation of pulmonary fibrosis. Respir Res 24: 296, 2023.
18. D'Alessandro-Gabazza CN, Yasuma T, Kobayashi T, Toda M, Abdel-Hamid AM, Fujimoto H, Hataji O, Nakahara H, Takeshita A, Nishihama K, *et al*: Inhibition of lung microbiota-derived proapoptotic peptides ameliorates acute exacerbation of pulmonary fibrosis. Nat Commun 13: 1558, 2022.
19. Cho SJ, Moon JS, Nikahira K, Yun HS, Harris R, Hong KS, Huang H, Choi AMK and Stout-Delgado H: GLUT1-dependent glycolysis regulates exacerbation of fibrosis via AIM2 inflammasome activation. Thorax 75: 227-236, 2020.
20. Liang J, Zhang Y, Xie T, Liu N, Chen H, Geng Y, Kurkciyan A, Mena JM, Stripp BR, Jiang D and Noble PW: Hyaluronan and TLR4 promote surfactant-protein-C-positive alveolar progenitor cell renewal and prevent severe pulmonary fibrosis in mice. Nat Med 22: 1285-1293, 2016.
21. Xie T, Liang J, Stripp B and Noble PW: Cell-cell interactions and communication dynamics in lung fibrosis. Chin Med J Pulm Crit Care Med 2: 63-71, 2024.
22. Huang G, Geng Y, Kulur V, Liu N, Liu X, Taghavifar F, Liang J, Noble PW and Jiang D: Arrestin beta 1 regulates alveolar progenitor renewal and lung fibrosis. J Respir Biol Transl Med 1: 10006, 2024.
23. Ashley SL, Jegal Y, Moore TA, van Dyk LF, Laouar Y and Moore BB: γ-Herpes virus-68, but not Pseudomonas aeruginosa or influenza A (H1N1), exacerbates established murine lung fibrosis. Am J Physiol Lung Cell Mol Physiol 307: L219-L230, 2014.
24. Kim MS, Kim SH, Jeon D, Kim HY, Han JY, Kim B and Lee K: Low-dose cadmium exposure exacerbates polyhexamethylene guanidine-induced lung fibrosis in mice. J Toxicol Environ Health A 81: 384-396, 2018.
25. D'Alessandro-Gabazza CN, Kobayashi T, Yasuma T, Toda M, Kim H, Fujimoto H, Hataji O, Takeshita A, Nishihama K, Okano T, *et al*: A Staphylococcus pro-apoptotic peptide induces acute exacerbation of pulmonary fibrosis. Nat Commun 11: 1539, 2020.
26. Yang L, Lin Z, Wang Y, Li C, Xu W, Li Q, Yao W, Song Z and Liu G: Nickle(II) ions exacerbate bleomycin-induced pulmonary inflammation and fibrosis by activating the ROS/Akt signaling pathway. Environ Sci Pollut Res Int 25: 4406-4418, 2018.
27. Chen S, Zhang X, Yang C, Wang S and Shen H: Essential role of IL-17 in acute exacerbation of pulmonary fibrosis induced by non-typeable Haemophilus influenzae. Theranostics 12: 5125-5137, 2022.
28. Kimura T, Nojiri T, Hosoda H, Shintani Y, Inoue M, Miyazato M, Okumura M and Kangawa K: Exacerbation of bleomycin-induced injury by lipopolysaccharide in mice: Establishment of a mouse model for acute exacerbation of interstitial lung diseases. Eur J Cardiothorac Surg 48: e85-e91, 2015.
29. Wei YR, Qiu H, Wu Q, Du YK, Yin ZF, Chen SS, Jin YP, Zhao MM, Wang C, Weng D and Li HP: Establishment of the mouse model of acute exacerbation of idiopathic pulmonary fibrosis. Exp Lung Res 42: 75-86, 2016.
30. Jia K, Wu J, Li Y, Liu J, Liu R, Cai Y, Zhang Y and Li X: A novel pulmonary fibrosis murine model with immune-related liver injury. Animal Model Exp Med 6: 274-282, 2023.
31. McMillan TR, Moore BB, Weinberg JB, Vannella KM, Fields WB, Christensen PJ, van Dyk LF and Toews GB: Exacerbation of established pulmonary fibrosis in a murine model by gammaherpesvirus. Am J Respir Crit Care Med 177: 771-780, 2008.
32. Hübner RH, Gitter W, El Mokhtari NE, Mathiak M, Both M, Bolte H, Freitag-Wolf S and Bewig B: Standardized quantification of pulmonary fibrosis in histological samples. Biotechniques 44: 507-511, 514-517, 2008.

33. Müller NL, Mawson JB, Mathieson JR, Abboud R, Ostrow DN and Champion P: Sarcoidosis: Correlation of extent of disease at CT with clinical, functional, and radiographic findings. Radiology 171: 613-618, 1989.
34. Livak KJ and Schmittgen TD: Analysis of relative gene expression data using real-time quantitative PCR and the 2(-Delta Delta C(T)) method. Methods 25: 402-408, 2001.
35. Konishi K, Gibson KF, Lindell KO, Richards TJ, Zhang Y, Dhir R, Bisceglia M, Gilbert S, Yousem SA, Song JW, *et al*: Gene expression profiles of acute exacerbations of idiopathic pulmonary fibrosis. Am J Respir Crit Care Med 180: 167-175, 2009.
36. Biondini D, Balestro E, Sverzellati N, Cocconcelli E, Bernardinello N, Ryerson CJ and Spagnolo P: Acute exacerbations of idiopathic pulmonary fibrosis (AE-IPF): An overview of current and future therapeutic strategies. Expert Rev Respir Med 14: 405-414, 2020.
37. Weng D, Chen XQ, Qiu H, Zhang Y, Li QH, Zhao MM, Wu Q, Chen T, Hu Y, Wang LS, *et al*: The role of infection in acute exacerbation of idiopathic pulmonary fibrosis. Mediators Inflamm 2019: 5160694, 2019.
38. O'Dwyer DN, Ashley SL, Gurczynski SJ, Xia M, Wilke C, Falkowski NR, Norman KC, Arnold KB, Huffnagle GB, Salisbury ML, *et al*: Lung microbiota contribute to pulmonary inflammation and disease progression in pulmonary fibrosis. Am J Respir Crit Care Med 199: 1127-1138, 2019.
39. Redente EF, Black BP, Backos DS, Bahadur AN, Humphries SM, Lynch DA, Tuder RM, Zemans RL and Riches DWH: Persistent, progressive pulmonary fibrosis and epithelial remodeling in mice. Am J Respir Cell Mol Biol 64: 669-676, 2021.
40. Zhao S, Wu X, Tan Z, Li L, Ou J, Lin Y, Song H, Feng L, Seto D, Wu J, *et al*: Generation of human embryonic stem cell-derived lung organoids for modeling infection and replication differences between human adenovirus types 3 and 55 and evaluating potential antiviral drugs. J Virol 97: e0020923, 2023.
41. Lynch JP and Kajon AE: Adenovirus: Epidemiology, global spread of novel types, and approach to treatment. Semin Respir Crit Care Med 42: 800-821, 2021.
42. Huang WJ and Tang XX: Virus infection induced pulmonary fibrosis. J Transl Med 19: 496, 2021.
43. Zhou Y, Jin T, Gao M, Luo Z, Mutahir S, Shi C, Xie T, Lin L, Xu J, Liao Y, *et al*: Aqueous extract of Platycodon grandiflorus attenuates lipopolysaccharide-induced apoptosis and inflammatory cell infiltration in mouse lungs by inhibiting PI3K/Akt signaling. Chin Med 18: 36, 2023.
44. Li J, Lu K, Sun F, Tan S, Zhang X, Sheng W, Hao W, Liu M, Lv W and Han W: Panaxydol attenuates ferroptosis against LPS-induced acute lung injury in mice by Keap1-Nrf2/HO-1 pathway. J Transl Med 19: 96, 2021.
45. D'Alessio FR: Mouse models of acute lung injury and ARDS. In: Alper S and Janssen W (eds), Lung Innate Immunity and Inflammation. Methods in Molecular Biology, vol 1809. Humana Press, New York, NY, pp341-350, 2018.
46. Seemann S, Zohles F and Lupp A: Comprehensive comparison of three different animal models for systemic inflammation. J Biomed Sci 24: 60, 2017.
47. Guo B, Liu W, Ji X, Xi B, Meng X, Xie W, Sun Y, Zhang M, Liu P, Zhang W, *et al*: CSF3 aggravates acute exacerbation of pulmonary fibrosis by disrupting alveolar epithelial barrier integrity. Int Immunopharmacol 135: 112322, 2024.
48. Pitre T, Lupas D, Ebeido I, Colak A, Modi M, Kachkovski GV, Montesi SB, Khor YH, Kawano-Dourado L, Jenkins G, *et al*: Prognostic factors associated with mortality in acute exacerbations of idiopathic pulmonary fibrosis: A systematic review and meta-analysis. Respir Med 222: 107515, 2024.
49. Moghoofei M, Mostafaei S, Kondori N, Armstrong ME and Babaei F: Bacterial and viral coinfection in idiopathic pulmonary fibrosis patients: The prevalence and possible role in disease progression. BMC Pulm Med 22: 60, 2022.
50. Yegen CH, Haine L, Da Costa Ferreira K, Marchant D, Bernaudin JF, Planès C, Voituron N and Boncoeur E: A new model of acute exacerbation of experimental pulmonary fibrosis in mice. Cells 11: 3379, 2022.
51. Fikry H, Saleh LA and Gawad SA: Therapeutic effect of adipose-derived mesenchymal stem cells (AD-MSCs) compared to pirfenidone on corticosteroid resistance in a mouse model of acute exacerbation of idiopathic pulmonary fibrosis. Histol Histopathol 37: 1065-1083, 2022.
52. Emura I and Usuda H: Acute exacerbation of IPF has systemic consequences with multiple organ injury, with SRA^+ and TNF-α^+ cells in the systemic circulation playing central roles in multiple organ injury. BMC Pulm Med 16: 138, 2016.
53. Papiris SA, Tomos IP, Karakatsani A, Spathis A, Korbila I, Analitis A, Kolilekas L, Kagouridis K, Loukides S, Karakitsos P and Manali ED: High levels of IL-6 and IL-8 characterize early-on idiopathic pulmonary fibrosis acute exacerbations. Cytokine 102: 168-172, 2018.
54. Li X, Zhou Y, Zou R, Chen H, Liu X, Qiu X, Xiao Y, Cai H and Dai J: Associations of serological biomarkers of sICAM-1, IL-1β, MIF, and su-PAR with 3-month mortality in acute exacerbation of idiopathic pulmonary fibrosis. Mediators Inflamm 2020: 4534272, 2020.
55. Tomos I, Dimakopoulou K, Manali ED, Papiris SA and Karakatsani A: Long-term personal air pollution exposure and risk for acute exacerbation of idiopathic pulmonary fibrosis. Environ Health 20: 99, 2021.